Article

Fission Mechanism of 235U+n Reaction According to the Symmetrical Atomic Nucleus Model

Vladimir A. Denisov [1], Vladimir P. Razinkin [2] and Victor V. Atuchin [3,4,5,6,*]

[1] Faculty of Radio Engineering and Electronics, Novosibirsk State Technical University, 630073 Novosibirsk, Russia
[2] Department of Theoretical Fundamentals of Radio Engineering, Novosibirsk State Technical University, 630073 Novosibirsk, Russia
[3] Laboratory of Optical Materials and Structures, Institute of Semiconductor Physics, SB RAS, 630090 Novosibirsk, Russia
[4] Research and Development Department, Kemerovo State University, 650000 Kemerovo, Russia
[5] Department of Industrial Machinery Design, Novosibirsk State Technical University, 630073 Novosibirsk, Russia
[6] R&D Center "Advanced Electronic Technologies", Tomsk State University, 634034 Tomsk, Russia
* Correspondence: atuchin@isp.nsc.ru

Abstract: In this study, the variants of structures are considered for fission fragments of the 235U nucleus caused by thermal neutrons, depending on differences in the initial configuration of proton, neutron and alpha particle compositions, according to a symmetrical model developed for the atomic nucleus. The proposed model is based on the principles of spatial symmetry and the analysis of the binding energy of the nucleus, taking into account the quark structure of nucleons. For the first time, the number of alpha particles in the composition of the 235U nucleus is considered to be 44 and the total number of connections between nucleons is 292. The work compares the binding energy of fragments of the atomic nucleus 235U, which have the same number of protons and neutrons in their composition, but a different number of alpha particles. The results obtained are the basis for an experimental study on the energy characteristics of various fission options of the 235U+n reaction, which is of interest for improving the efficiency of nuclear power sources.

Keywords: fission; 235U; symmetric model nuclei; binding energies nuclei; olgoid

1. Introduction

Forced fission of isotopes of heavy mass elements by interaction with thermal neutrons is a complex and multi-factor process. In studying this process, many authors have aimed at developing and describing the fission mechanism [1–13], sets of the most probable fission fragments [14–19] and elementary particles [20–22], and total energy balance [23–28].

In an atomic nucleus, neutrons and protons are equally subject to short-range nuclear forces that attract nucleons to each other at a distance of around 1 femtometer. Nuclear forces ensure long-term stability of atomic nuclei due to a high nuclear potential of about 50 MeV. The short-range nuclear forces are also characterized by charge independence. The nuclear forces have a saturation property, meaning that the nucleon in a nucleus can interact only with a limited number of adjacent nucleons. That is why the dependence of nuclei binding energies on their mass numbers is linear. Almost complete saturation of nuclear forces is achieved for the A-particle, which is stable.

In the present study, we consider the thermal neutron-induced fission of 235U because it is the best way to study the structure of the initial isotope without a substantial breakage of internal nucleon associations in the nucleus. Higher energies of the nuclear excitation (by fast neutrons, gamma radiation, fragments with high kinetic energy) substantially affect the nucleus thin structure. Such effects are established and described in detail in Ref. [11].

Investigations and descriptions of nucleus binary fission by thermal neutrons can also be found in the literature [29–32]. However, the representation in these papers does not reflect the internal nucleus structure in the fission mechanism. Delayed ternary and quaternary atomic nuclei fissions have been considered in the literature [33–36]. It should be pointed out that fissions of these types are, in essence, decay processes of the fragments produced after binary fission, so they can be combined with the results of contributions on nuclei decays [37].

The reliability of the description of the 235U+n fission mechanism is, to a great extent, determined by the choice of nucleus model. However, at present, none of the many proposed atomic nucleus models can completely explain all existing experimental data. It is worth noting that one of the first models introduced was the collective "Droplet model" (DM), in which the atomic nucleus was represented as a spherical droplet consisting of nuclear substances [38]. Using empirical relations, energy parameters of nuclei were determined for 235U [38]. However, it is not possible, in principle, within this model, to describe the internal microscopic components in an atomic nucleus and the types of their interaction and to explain the high stability of some heavy nuclei. In addition, the model does not allow for reliable prediction and analysis of the compositions of light and heavy fragments in the nuclear fission reaction of 235U.

Later, a microscopic shell model was developed, termed the "independent-particle model" (IPM) or "shell model" (SM) [39], where the nucleus was considered as a system of interacting nucleons creating an internal force field and each of the nucleons is in a certain quantum state characterized by energy and angular momenta. Sets of nucleons with close energy states form a corresponding nucleus energy shell. Transfer to the next shell is carried out according to the Pauli principle that does not allow two equal fermions to occupy the same shell. This model led to the introduction of the nucleus properties periodicity hypothesis, but attempts to provide a rigorous and systematic description of all chemical element nuclei encountered great mathematical difficulties [39]. Within this model, it is not possible to accurately determine the point at which breakage in the nucleus structure during fission will take place because nucleus shells are in continuous dynamic interaction with each other.

The next step in the study of atomic nuclei properties was the development of the "cluster model" (CM) [39–41] and the "close-packed-spheron model" (CPSM) [42,43]. These models assume that a nucleus consists of alpha-particle clusters. Such an approach allows for visualization of the internal spatial structure of the nucleus and to obtain a good match between the calculated and experimental data for chemical elements with low ordinal numbers. However, for high-atomic-weight elements (over 16), these models have not been well developed, since an alpha particle is not considered as an element of the nucleus structure with a fixed binding energy value.

The common drawback of all the above-mentioned models is that they do not provide an exact location in the nucleus where structural breakage takes place and what fragment structures are grouped into fission product isomers. All known models a priori assume a random position of the breakage between nucleons.

To overcome the above-mentioned drawbacks, we propose, in the present paper, a symmetrical atomic nucleus model termed the "symmetric model nuclei" (SMN) developed on the basis of the fundamental symmetry properties of atomic nuclei [44]. The unique feature of the proposed model is the progression from a mathematical description of nucleus symmetry to the construction of spatially symmetrical structures of atomic nuclei with appropriate bindings of nucleons. When forming symmetrical spatial structures, it is assumed that nucleons may bind with no more than three other nucleons within the nucleus. This limitation is one of the principal foundations of the SMN model and complies with the requirements for inter-nucleon bindings described in Ref. [45]. In addition, within the SMN model, the quark structure of nucleons is substantiated and taken into consideration as well as binding energy analysis being provided.

Thus, in the present work, the 235U+n nucleus fission mechanism is considered by means of the SMN model, where it is assumed that nucleons inside a nucleus are symmetrically ordered in space. The main advantage of the proposed model is a structural description of the physical mechanism of fission. It allows for predicting the most probable fragment structures and probable types of atomic nucleus isomers, in particular, for the 235U isotope. An important good property of the SMN model is high description accuracy of heavy nucleus decay process, fragment synthesis and predicting new structures.

The SMN model is based on the following initial statements:

An atomic nucleus consists of protons, neutrons and alpha particles. Alpha particles are individual components with a fixed internal binding energy.

Alpha particles, protons and neutrons in a nucleus form a symmetrically ordered three-dimensional structure. Analysis of the 235U atomic nucleus structure revealed that the thermal neutron-induced fission of the nucleus produces two approximately equal mass fragments, where strictly definite links between nucleons are broken.

Nuclear attraction and repulsion forces act between all the components of a nucleus. These forces ensure the dynamic stability of a nucleus.

The chosen approach to the investigation and c decoding of nucleus spatial structures via the analysis of binding energy based on the SMN model has shown that an alpha particle is a separate independent type of particle in a nucleus structure, together with a proton and neutron. It has a constant binding energy of helium four nucleus-B_S(4He) ≈ 28.296 MeV. This energy does not depend on an alpha-particle position: in the nucleus center, on the periphery or it is associated with other nucleons and alpha particles. This effect can be characterized as a confinement of an alpha particle, which can be destroyed by the excitation energy exceeding the given threshold. When an alpha particle is destroyed, new associations consisting of two protons and two neutrons with a far lower binding energy appear. Here, the quark structure of alpha particles is also taken into account. In the SMN model diagrams, each alpha particle is denoted as "A" particle and position of the character "A" carries the information about the internal bindings of quarks. Therefore, the investigation of the 235U+n nucleus fission mechanism is an important element of the chain of proof of symmetrically ordered properties of an atomic nuclei. That is the essence of the new approach to the nucleus binding energy analysis. The SMN model clearly explains an internal structure of 235U, taking into account all known factors. This model considers, in a new way, the nucleus fission to two approximately equal fragments along a strictly definite line, shifted from the geometric center of the nucleus. The difference in the fragment nucleon link structure in fission products can be explained by the different external particle attachments to the nucleus periphery that points to the structure difference between isomers of the same 235U isotope. The results of these investigations will provide an adequate theoretical basis for explaining the available experimental data.

2. Brief Characteristics of Symmetrical Atomic Nucleus Model

The basic equation of the SMN model is the formula for the nucleus binding energy calculation $B_S(X)$ (X denotes an isotope of an element, where each alpha particle contributes the fixed value of the binding energy B_S (He4) to the total binding energy of the nucleus X:

$$B_S(X) = (Z - 2 \cdot N_A) \cdot m_p \cdot C^2 + (N - 2 \cdot N_A) \cdot m_n \cdot C^2 + N_A \cdot (m_A \cdot C^2 + B_S(4He)) - M_S(X) \cdot C^2, \quad (1)$$

where Z is the number of protons; N is the number of neutrons; N_A is the number of "A" particles; m_p is the proton mass; m_n is the neutron mass; m_A is the mass of "A" particle ($m_A \cdot C^2 = 2 \cdot m_p \cdot C^2 + 2 \cdot m_n \cdot C^2 - B_S(4He)$); $M_S(X)$ is the mass of nucleus X; C is the light speed.

The general formula of the binding energy for a particular nucleus X has the form

$$B_S(X) = B_A(X) + B_C(X), \quad (2)$$

where $B_A(X)$ is the internal binding energy contributed by all "A" particles and equal to $B_A(X) = N_A \cdot B_S(4He)$; $B_C(X)$ is the binding energy contributed by all bindings between protons, neutrons and "A" particles in the particular nucleus X.

The maximal possible force of a nucleon–nucleon interaction inside an "A" particle is determined by the binding energy $B_S(4He) \approx 28.296$ MeV. A quark structure of nucleons (consisting of three quarks) is taken into account as well as the capability of nucleons to have no more than three links with adjacent nucleons [45]. It follows from these conditions that the "A" particle must have four internal links between two protons and two neutrons that may be denoted as "A-type" links. Hence, the average binding energy per "A-type" link is approximately $B_S(4He)/4 \approx 28.296/4 \approx 7.074$ MeV. Only when all four "A-type" links of an "A" particle are broken simultaneously, the "A" particle will decay. In this case, the nucleons will form less strong "C-type" links. Therefore, it is necessary to know how many "A" particles are in a nucleus in order to calculate the nucleus binding energy. The main distinction between the "A-type" and "C-type" links is that "A-type" links have the maximal average binding energy per link, about 7.074 MeV, whereas "C-type" links have a varying and always lower than the 7.074 MeV value of the average binding energy per link for any kind of atomic nucleus.

For a visual representation of nucleon interaction, it is convenient to introduce a special image of atomic nucleus internal structure that we named as "olgoid". These diagrams allow for a visual analysis of the links between nucleons and monitor interaction reactions of nucleon–nucleon forces. In the nucleus structural diagrams, it is convenient to denote the alpha particle (nucleus 4He) with capital letter "A" (alpha) of the Greek alphabet. This allows for picturing heavy nuclei structures that contain "A" particles without overloading the diagram by secondary details. The examples of "olgoid" diagrams for several nuclei of stable chemical elements are represented in Figures 1 and 2. We observed that when the chemical element ordinal number is increased, the links between nucleons and "A" particles are formed in a symmetrically ordered way, with respect to the basic principles of the SMN model. Therefore, this model is associated with the atomic nucleus symmetry discovered by Wigner in 1937 [44]. That is why the model was named the symmetrical atomic nucleus model or "Symmetric model nuclei" (SMN). The main characteristics of "olgoids" shown in Figures 1 and 2 are presented in Table 1. In addition to the main characteristics of olgoids, Table 1 contains some additional parameters: N_{cC} is the number of "C-type" links; $N_{cS} = N_{cA} + N_{cC}$ is the total number of links between nucleons in a nucleus, where $N_{cA} = N_A \cdot 4$ is the number of "A-type" links. A more detailed description of the rules for constructing an "olgoid" is out of the scope of the present paper. The "A-type" links are shown as red lines between nucleon "A" particles (in the colored picture) and "C-type" links are shown as black lines between protons, neutrons and "A" particles. Protons are shown in green color and neutrons are in white.
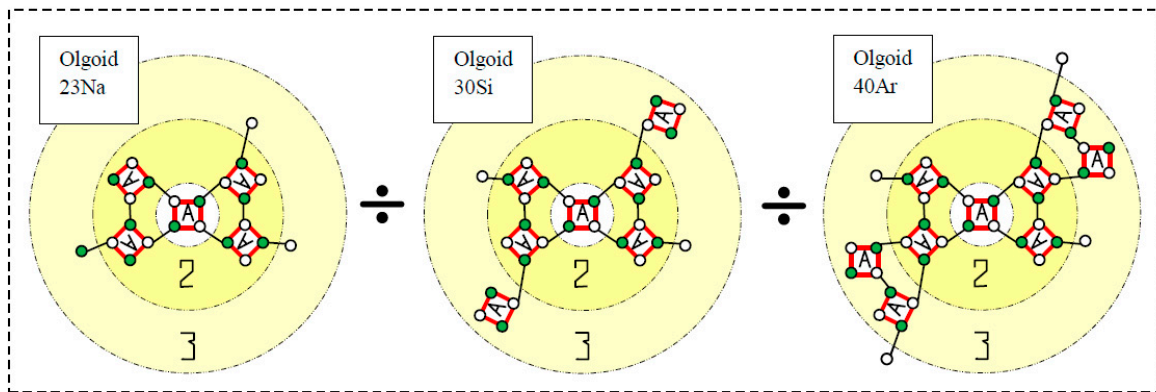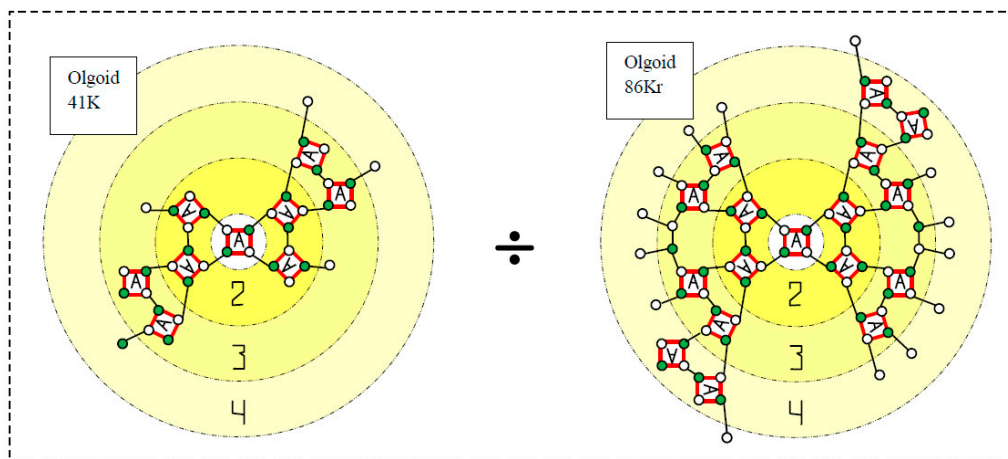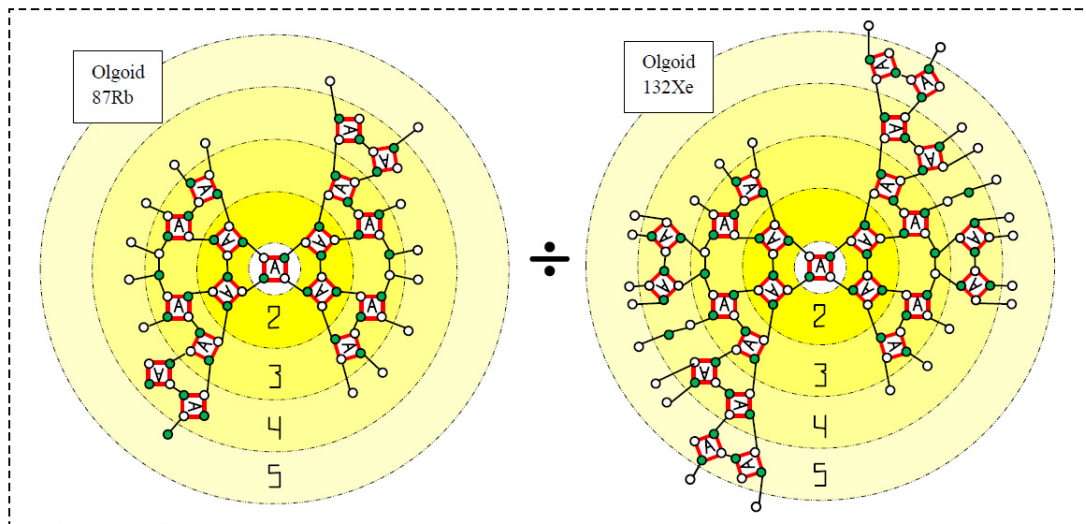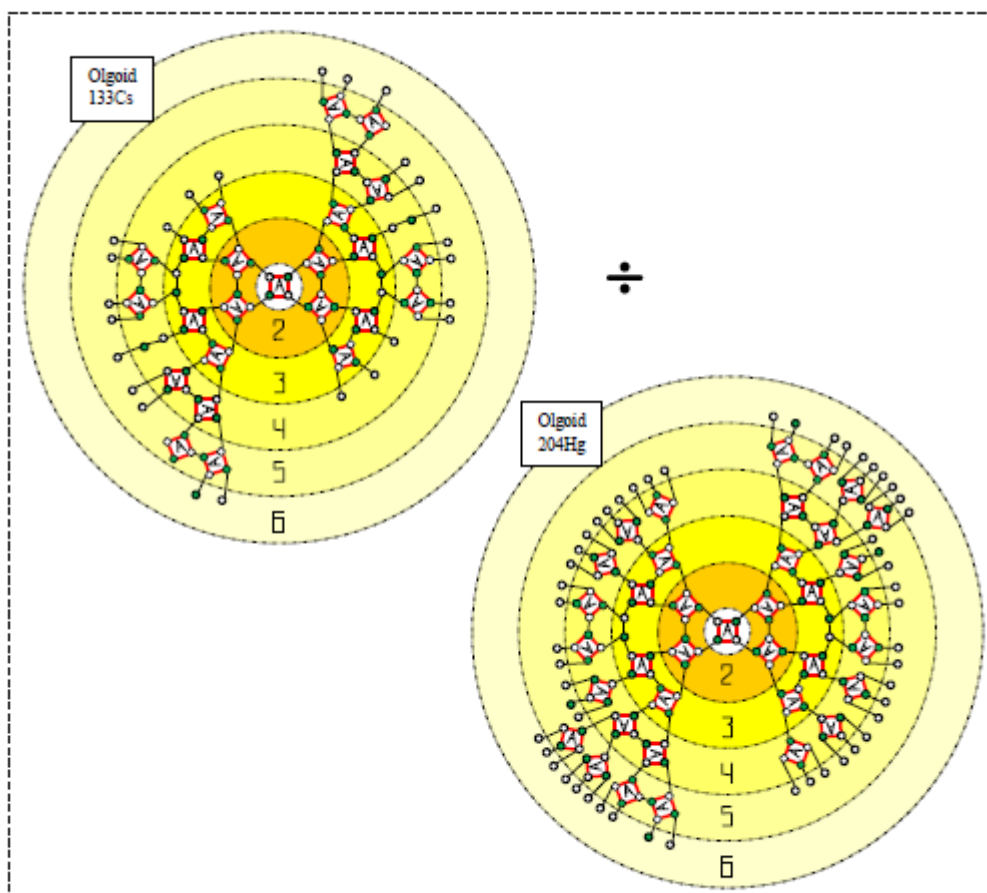

a

Figure 1. *Cont.*
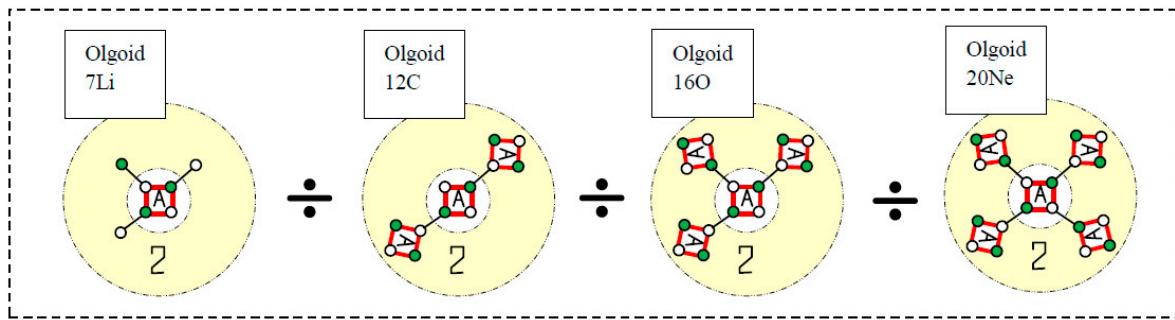
b

c

d

Figure 1. Nucleus structures of stable chemical element isotopes: first (**a**), second (**b**), third (**c**) and fourth (**d**) periods of D. I. Mendeleyev periodic table of elements.

a

b

Figure 2. Nucleus structures of stable chemical element isotopes: fifth (**a**) and sixth (**b**) periods of the D. I. Mendeleyev periodic table of elements.

Table 1. Main characteristics of "olgoids" shown in Figures 1 and 2.

| Olgoid	Z	N	B_S	N_A	B_A	$B_C = B_S - B_A$	N_{cC}	B_C/N_{cC}	N_{cS}
			MeV		MeV	MeV		MeV	
1H	1	0	0	0	0	0	0	0	0
4He	2	2	28.296	1	28.296	0	0	0	4
7Li	3	4	39.244	1	28.296	10.948	3	3.649	7
12C	6	6	92.162	3	84.888	7.274	2	3.637	14
16O	8	8	127.619	4	113.183	14.436	3	4.812	19
20Ne	10	10	160.645	5	141.478	19.167	4	4.792	24
23Na	11	12	186.564	5	141.478	45.086	9	5.009	29
30Si	14	16	255.620	7	198.07	57.55	10	5.755	38
40Ar	18	22	343.810	9	254.661	89.149	16	5.572	52
41K	19	22	351.619	9	254.661	96.958	17	5.703	53
86Kr	36	50	749.234	17	481.026	268.208	44	6.096	112
85Rb	37	48	739.282	16	452.731	286.551	46	6.229	110
87Rb	37	50	757.856	17	481.026	276.830	45	6.152	113
89Rb	37	52	771.113	17	481.026	290.087	47	6.172	115
91Rb	37	54	783.288	17	481.026	302.262	49	6.169	117
132Xe	54	78	1112.448	25	707.392	405.056	70	5.787	170
133Cs	55	78	1118.527	25	707.392	411.135	71	5.791	171
204Hg	80	124	1608.651	37	1046.939	561.712	106	5.299	254
235U	92	143	1783.86	44	1245.02	538.836	116	4.645	292
238U	92	146	1801.69	45	1273.32	528.37	116	4.555	296

Based on the analysis of the structures of known nuclides, we modeled the most probable structure of the 235U_a nucleus shown in Figure 3a. According to (1) and (2), this structure has the following parameters: B_S(235U_a) = 1783.86 MeV; Z = 92; N = 143; N_A = 44; B_A(235U_a) = 1245.024 MeV; B_C(235U_a) = 538.836 MeV. It is useful to know the additional parameters of the 235U_a nucleus structure: $N_{cA} = N_A \cdot 4 = 176$ is the number of "A-type" links; $N_{cC} = 116$ is the number of "C-type" links; and $N_{cS} = 292$ is the total number of links between nucleons in the nucleus.

However, in addition to the structure shown in Figure 3, there might be configurations with slightly different links of protons, neutrons and "A" particles that are isomers to the most probable structure of the nucleus. Six similar structures for the 235U nucleus are shown in Figures 3 and 4. They are denoted as "olgoids" 235U_a, 235U_b, 235U_c, 235U_d, 235U_e and 235U_f, respectively. Two "olgoid" groups, a, b, c and d, e, f, will form fragments with even or odd numbers of protons. There exist less probable "olgoid" 235U configurations, but these six are the most compatible with the SMN model rules.

As follows from the analysis of the SMN, when energies of affecting neutrons exceed 10 MeV, the breakage occurs in the center of a nucleus where the central "A" particle resides. In that case, the particle decays because its nucleons cannot transfer such high energies from one half of the nucleus to another. Therefore, the nucleus is divided into approximately equal fragments, appropriate for the given energy of affecting protons and it is proved experimentally.
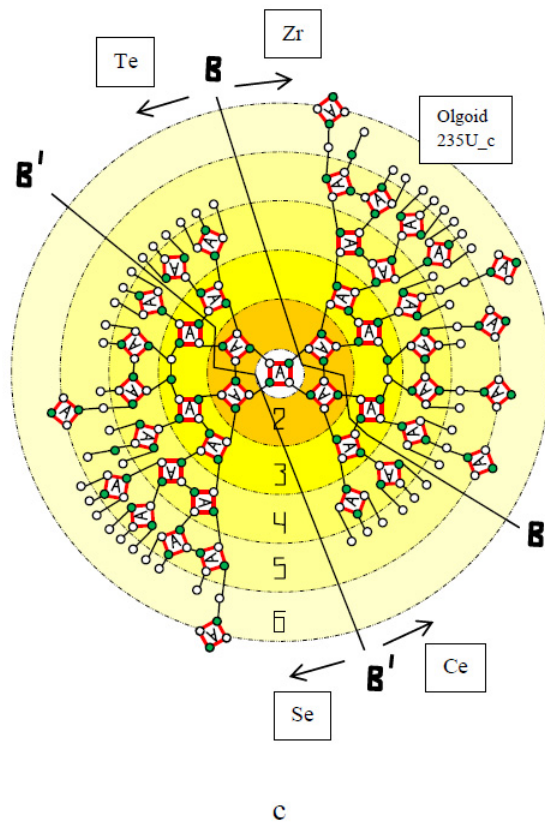
a

b

Figure 3. *Cont.*

c
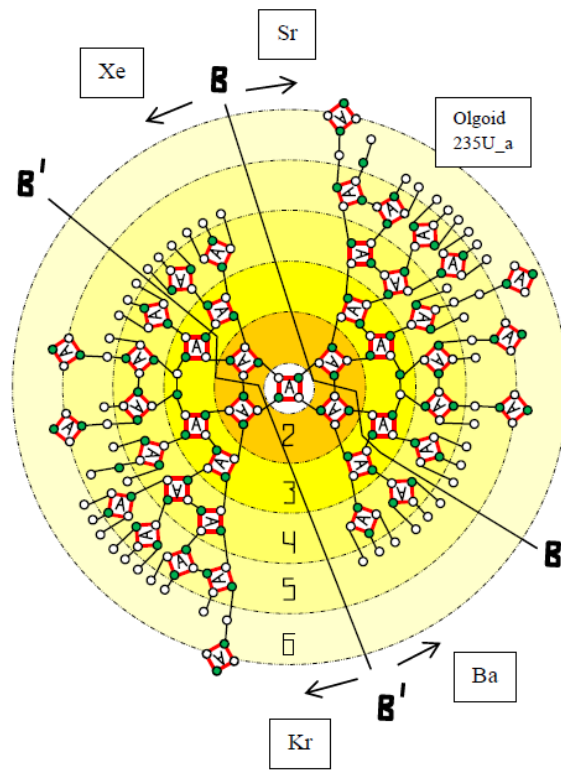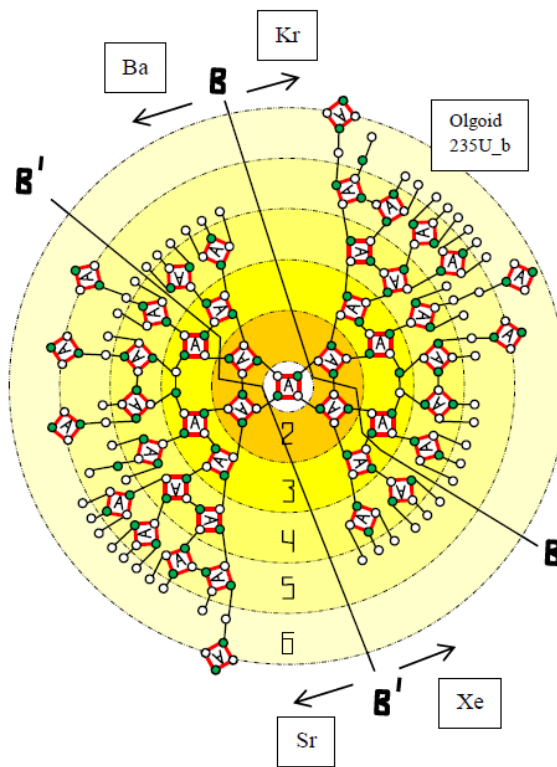
Figure 3. Fission into fragments with the even number of protons for "olgoids" 235U_a (**a**), 235U_b (**b**), 235 U_c (**c**) along line B-B or B′-B′.

Figure 4. *Cont.*

b

c
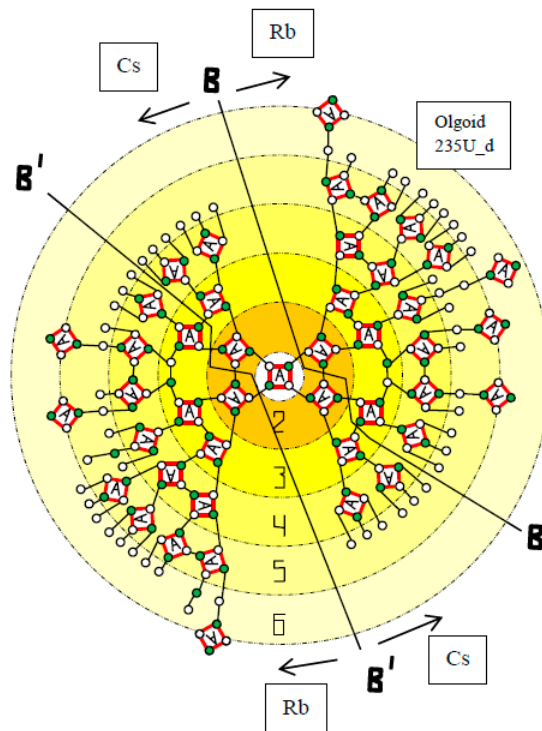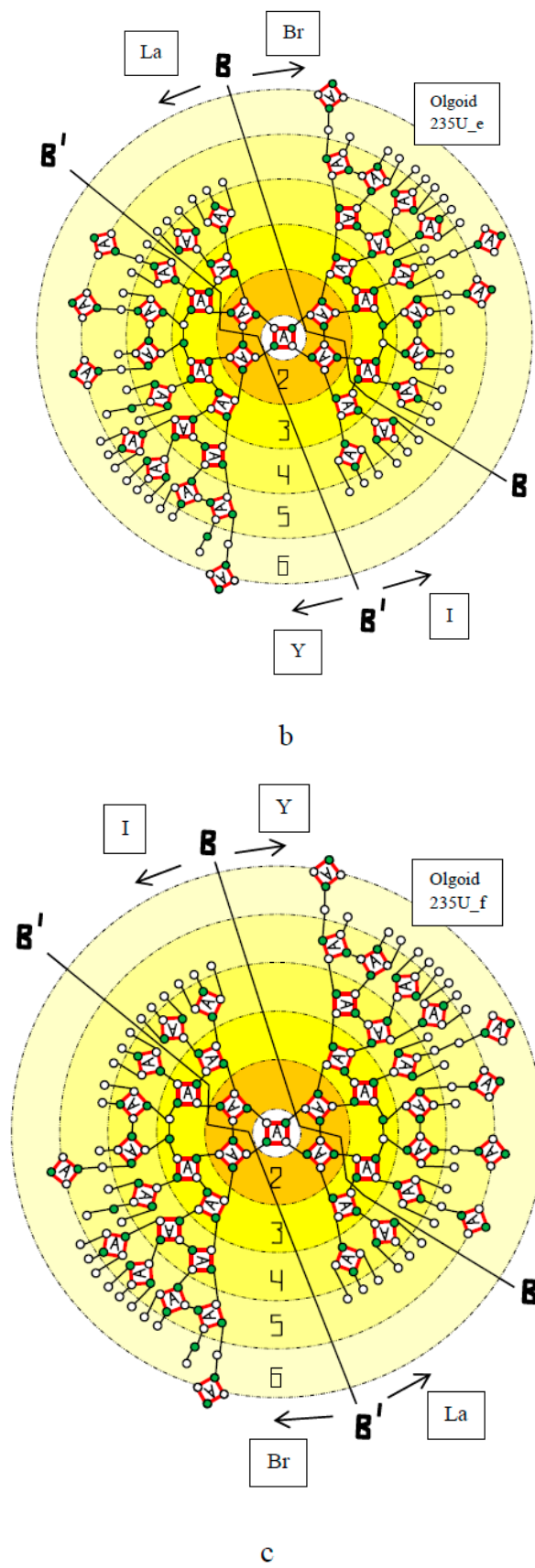
Figure 4. Fission into fragments with the odd number of protons for "olgoids" 235U_d (**a**), 235U_e (**b**), 235U_f (**c**) along line B-B or B′-B′.

3. 235U Nucleus Reaction Fission Mechanism

Our proposed approach to the description of the 235U+n nucleus fission consists of three stages: (1) definition of equations describing the reactions of the 235U+n nucleus fission along the most probable lines of the nucleus breakage; (2) description of the fission into less probable fragments and (3) consequences and predictions.

3.1. Equations of 235U Nucleus Fission Reactions

The fission of "olgoids" 235U_a, 235U_b, 235U_c, 235U_d, 235U_e and 235U_f along the breakage line B-B to the right of the nucleus center and along the line B′-B′ to the left of the nucleus center is shown in Figures 3 and 4. The most probable fission along the lines B-B and B′-B′ can be explained by the structure of the "olgoid" 235U and the results of modeling lighter nuclei. It can be seen in Figures 3 and 4 that the "olgoid" consists of three basic parts: the middle part centered at the first layer (layers are marked with dotted circle lines and are colored with different shades of yellow) and the two approximately similar lobes. The lobe on the right is separated from the center by the B-B line and a similar lobe is on the left and is separated from the center by the B′-B′ line. The lobes of the "olgoid" 235U tend to take a part of the nucleus binding energy from the center in order to form their own centers of binding energy concentration and create their own nucleus. Due to this, heavy element nuclei are relatively unstable and internal forces tend to break them as well as the binding energy per nucleon decreases with an increase in nucleon number. The "A" particle residing in the center in the first layer tends to prevent peripheral groups of nucleons from separation. About 6 MeV of critical energy is enough to start the separation of the "olgoid" 235U lobes. In this case, the nucleus breaks not by halves, but in two different but similar mass fragments. The energy balance of 235U nucleus fission by thermal neutrons is represented in Table 2 [38]. The fission product yield is given in Table 3 [46], where the following notation is used: A is the atomic mass number; Y(A) is the fission isomer yield for all nuclides with the atomic mass number of A; Y(X) is the fission yield for the most probable nuclide X; τ(X) is the period of half-decay for the nuclide X.

Table 2. Fission energy distribution for the U235 nucleus fission by thermal neutrons [38].

Kinetic Energy of Fragments	167 MeV
Kinetic energy of neutrons	5 MeV
Electrons of β-decay of fission products	7 MeV
Anti-neutrino of β-decay of fission products	9 MeV
Instantaneous γ-radiation	8 MeV
γ-radiation of fission products	7 MeV
Total energy of fission	203 MeV

The fission mechanism for the right lobe is determined by the breakage in the lower part (Figures 3 and 4) of the line B-B in the weakest link between the "A" particles of the 3rd layer of protons. At this moment, the redistribution of the 200 MeV nucleus binding energy between the fragments begins. Then, the links between the "A" particles of the 3rd and 2nd layers break, the links between "A" particles of the 2nd layer break and, finally, the strongest link between "A" particles of the 2nd and 1st proton layers breaks. Further, two or three neutrons carry away a part of the energy in the way of fragment cooling. The fission mechanism for the left lobe is caused by the breakage of the upper part of the B′-B′ line (Figures 3 and 4) in the same sequence. The breakage appears between the weakest "A" particle links in the 3rd proton layer. Then, there begins the breakage between the "A" particles of the 3rd and the 2nd layers; after that, the breakage of the links between "A" particles and, finally, two or three neutrons carry away part of the energy. The "olgoids" 235U_a, 235U_b, 235U_c shown in Figure 3 are separated by the line B-B or B′-B′ in two fragments with an even number of protons. The "olgoids" 235U_d, 235U_e and 235U_f shown in Figure 4 are separated by the line B-B or B′-B′ in two fragments with an odd number of protons. For the separation of the "olgoid" 235U_a (Figure 3a) along the line

B-B, two variants are possible for the thermal neutron attachment to the right or to the left fragment.

Table 3. Fission product yield for the U235 nucleus fission by thermal neutrons [46].

(a) Light Fragments					(b) Heavy Fragments				
A	Y(A) %	Nuclide X	Y(X) %	t(X)	A	Y(A) %	Nuclide X	Y(X) %	t(X)
76	0.003	76Zn	0.0018	5.7s	118	0.011	118Ag	0.0064	4.0s
77	0.008	77Ga	0.0041	13c	119	0.013	119Ag	0.0073	2.1s
78	0.021	78Ga	0.0103	5.1s	120	0.013	120Cd	0.0084	51s
79	0.045	79Ge	0.0233	19s	121	0.013	121Cd	0.0072	13.5s
80	0.129	80Ge	0.102	29.5s	122	0.016	122Cd	0.012	5.3s
81	0.204	81Ge	0.126	7.6s	123	0.016	123Cd	0.010	2.1s
82	0.325	82As	0.129	19s	124	0.027	124Cd	0.012	1.24s
83	0.535	83As	0.291	13.4s	125	0.034	125Sn	0.011	9.63d
84	1.00	84Se	0.631	3.3s	126	0.059	126Sn	0.045	0.1My
85	1.32	85Se	0.894	39s	127	0.157	127Sn	0.095	2.1h
86	1.95	86Ge	0.629	0.25s	128	0.35	128Sn	0.301	59m
87	2.56	87Br	1.27	56s	129	0.79	129Sn	0.43	6.9m
88	3.58	88Kr	1.73	2.84h	130	1.18	130Sn	1.08	3.7m
89	4.74	89Kr	3.44	3.15m	131	2.89	131Sb	1.65	39s
90	5.78	90Kr	4.40	32.3s	132	4.31	132Sb	2.16	4.2m
91	5.83	91Kr	3.16	8.6s	133	6.70	133Te	4.14	55.4m
92	6.01	92Rb	3.13	4.5s	134	7.84	134Te	6.22	42m
93	6.36	93Rb	3.07	5.85s	135	6.54	135Te	3.22	19s
94	6.47	94Sr	4.51	1.25m	136	6.32	136I	2.57	1.39m
95	6.50	95Sr	4.54	25.1s	137	6.19	137Xe	3.19	3.82m
96	6.27	96Sr	3.57	1.06s	138	6.71	138Xe	4.81	14.1m
97	6.00	97Y	3.14	3.76s	139	6.41	139Xe	4.32	39.7s
98	5.76	98Zr	2.57	30.7s	140	6.22	140Xe	3.51	13.6s
99	6.11	99Zr	3.58	2.2s	141	5.85	141Cs	2.92	25s
100	6.29	100Zr	4.98	7.1s	142	5.84	142Ba	3.01	10.7m
101	5.18	101Zr	2.79	2.1s	143	5.95	143Ba	4.10	14.3s
102	4.29	102Zr	1.78	2.9s	144	5.50	144Ba	3.98	11.4s
103	3.03	103Nb	1.41	1.5s	145	3.93	145La	1.92	24s
104	1.88	104Mo	1.13	60s	146	3.00	146La	1.49	6.3s
105	0.96	105Mo	0.668	36s	147	2.25	147Ce	1.00	56s
106	0.402	106Mo	0.359	8.4s	148	1.67	148Ce	1.24	56s
107	0.146	107Mo	0.121	3.5s	149	1.08	149Ce	0.70	5.2s
108	0.054	108Mo	0.030	1.5s	150	0.653	150Ce	0.39	4.4s
109	0.031	109Mo	0.0155	1.4s	151	0.419	151Pr	0.24	22s
110	0.025	110Tc	0.012	0.83s	152	0.267	152Nd	0.141	11.4m
111	0.018	111Ru	0.012	1.5s	153	0.158	153Nd	0.111	29s
112	0.013	112Ru	0.0099	4.5s	154	0.074	154Nd	0.058	26s
113	0.014	113Rh	0.0064	2.7s	155	0.032	155Nd	0.018	8.9s
114	0.012	114Rh	0.0050	1.8s	156	0.014	156Pm	0.0071	27s
115	0.012	115Rh	0.0036	0.99s	157	0.006	157Pm	0.0029	11s
116	0.013	116Pd	0.0068	12.7s	158	0.003	158Sm	0.0024	5.5s
117	0.008	117Ag	0.0030	1.2m	159	0.001	Sm159	0.0007	11c

In the first variant, the thermal neutron attaches to the right strontium fragment, then the transient process, initiated by the thermal neutron, can result in various nuclear reactions, depending on which of the fragments has a higher excitation energy at the moment of the fragment separation. It depends on how many instantaneous neutrons are thrown away from the fragment: three, two, one or zero. In the present work, we show examples for the detachment of two instantaneous neutrons in order to represent the principal channel of 235U+n nucleus fission. It is possible to extend the analysis to the detachment of three instantaneous neutrons.

(a) If all excitation energy is concentrated in the strontium fragment, then two instantaneous neutrons will detach from it and the reaction equation is $235U\_a+1n \rightarrow 139Xe + (95Sr+2n)$, where: $1n$ is the thermal neutron in the left side of the equation; $2n$ are two instantaneous neutrons carrying away energy from the strontium fragment in the right side of the equation. $(95Sr+2n)$ is in parentheses to focus on this fragment. The total fragment yield, according to nuclide atomic mass number, is represented in Table 3.

(b) The excitation energy is distributed in both xenon and strontium fragments. In this case, each fragment detaches one instantaneous neutron according to equation $235U\_a+1n \rightarrow (138Xe+1n) + (96Sr+1n)$.

(c) All excitation energy is concentrated in the xenon fragment; therefore, it detaches two instantaneous neutrons and the reaction equation becomes $235U\_a+1n \rightarrow (137Xe+2n) + 97Sr$. In the data from Table 3, the strontium $97Sr$ fragment yield is not presented, but the most probable yttrium $97Y$ fragment yield is given. Hence, the delayed β-decay reaction $97Sr \rightarrow 97Y+e$, where e is an electron, is possible.

The second variant is when the thermal neutron attaches to the left xenon fragment. The following reactions are possible: (a) $235U\_a+1n \rightarrow 140Xe + (94Sr+2n)$; (b) $235U\_a+1n \rightarrow (139Xe+1n) + (95Sr+1n)$; (c) $235U\_a+1n \rightarrow (138Xe+2n) + 96Sr$. The fission product yields of these reactions comprise part of the data in Table 3.

The next "olgoid" $235U\_b$ is represented in Figure 3b. It differs from the already considered "olgoid" $235U\_a$ by the fact that one "A" particle slightly disturbs the "olgoid" symmetry by the attachment to the left lobe of the "olgoid" $235U\_a$ rather than to the right lobe. In the SMN model, the symmetry of the structure, with respect to the center, is an important nucleus parameter. The line of breakage B-B divides the "olgoid" into other fragments, namely barium and krypton. The equations of nuclear fission reactions, in this case, are similar to the already considered equations.

The first variant is when thermal neutron attaches to the right krypton fragment. The following reactions are possible: (a) $235U\_b+1n \rightarrow 143Ba + (91Kr +2n)$; (b) $235U\_b+1n \rightarrow (142Ba+1n) + (92Kr+1n)$. In Table 3, the fragment $92Kr$ yield is not mentioned, but the most probable fragment $92Rb$ is presented. Hence, the delayed β-decay reaction $92Kr \rightarrow 92Rb+e$ is possible. In this case: $235U\_b+1n \rightarrow (141Ba+2n) + 93Kr$. In Table 3, the fragment $93Kr$ yield is not mentioned, but the most probable fragment $93Rb$ is presented; therefore, the β-decay reaction $93Kr \rightarrow 93Rb+e$ is possible. In addition, in Table 3, the fragment barium $141Ba$ yield is not mentioned, but the most probable fragment cesium $141Cs$ is presented. Then, the reaction $141Ba+e \rightarrow 141Cs$ is possible.

The second variant is when the thermal neutron attaches to the left barium fragment. The following reactions are possible: (a) $235U\_b+1n \rightarrow 144Ba + (90Kr+2n)$; (b) $235U\_b+1n \rightarrow (143Ba+1n) + (91Kr+1n)$; (c) $235U\_b+1n \rightarrow (142Ba+2n) + 92Kr$. According to the above reasons, the reaction $Kr92 \rightarrow Rb92+e$ is possible.

The next "olgoid" $235U\_c$ is represented in Figure 3c. Its difference from that considered before "olgoid" $235U\_a$ is in the break of nucleus symmetry that occurs, owing to the attachment of one "A" particle to the right lobe of the "olgoid" $235U\_a$ instead of the left lobe. Thus, the breakage line B-B divides the "olgoid" into fragments of tellurium and zirconium. In this case, two variants of equations are possible.

The first variant is when a thermal neutron attaches to the right zirconium fragment. The following reactions are possible: (a) $235U\_c+1n \rightarrow 135Te + (99Zr+2n)$; (b) $235U\_c+1n \rightarrow (134Te+1n) + (100Zr+1n)$; (c) $235U\_c+1n \rightarrow (133Te+2n) + 101Zr$.

The second variant is when the thermal neutron attaches to the left tellurium fragment. The following reactions are possible: (a) $235U\_c+1n \rightarrow 136Te + (98Zr+2n)$. In Table 3, the fragment $Te136$ yield is not mentioned, but the most probable fragment $I136$ is presented and the reaction of β-decay $136Te \rightarrow 136I+e$ is possible. (b) $235U\_c+1n \rightarrow (135Te+1n) + (99Zr+1n)$. (c) $235U\_c+1n \rightarrow (134Te+2n) + 100Zr$.

In Figure 4a, "olgoid" $235U\_d$ fission along the B-B line is observed. In this case, the fragments of rubidium and cesium are created. According to the described scheme,

two variants for the thermal neutron attachment and instantaneous neutron detachment are possible.

The next "olgoid" 235U_e is represented in Figure 4b. The breakage line B-B divides the "olgoid" into lanthanum and bromine fragments. The "olgoid" 235U_f is also shown in Figure 4c. The breakage line B-B divides the "olgoid" on iodine and yttrium fragments. The fission procedures for different variants are repeated. All particular fragments with probabilities not equal to zero are listed in Table 3.

In Figures 3 and 4, the fission of the mentioned "olgoids" along the line B′-B′ is observed. It results in the following fragments: 235U_a-krypton and barium; 235U_b-strontium and xenon; 235U_c-selenium and cerium; 235U_d-rubidium and cesium; 235U_e-yttrium and iodine; 235U_f-bromine and lanthanum. Each fission has two variants of the thermal neutron attachment to the initial nucleus "olgoid"; the reactions of instantaneous neutron detachment remain analogous to those considered before.

3.2. 235U Nucleus Fission Reaction into Less Probable Fragments

In addition to the above-considered fragments, yields of less probable fission fragments are presented in Table 3 [46]. The data indicate the existence of two processes. The first one is characterized by the decay of the already considered fragments. The second one is characterized by the capture of various particles by the mentioned fragments. The instance of the first process for light fragments can be the "olgoid" 81Ge, shown in Figure 5a, which is obtained from the 85Se fragment (Figure 3) that has t(85Se) = 39 s (t(X) is the half-life period of nuclide X). In the case of alpha-decay, with the detachment of the "A" particle, the reaction equation is 85Se → 81Ge+4He. Yield Y(81Ge) = 0.126 (%) (Y(X) is the yield of the particular isotope X), Table 3. Such a process is defined in [33] as the ternary nucleus fission, where the third particles are emerging as secondary particles from the primary fragments of true binary fission. "Ternary nucleus fission" is a relatively rare (from 0.2% to 0.4% of cases) type of nucleus fission when three charged fragments, three new nuclei, are created. In usual fission, two charged fragments (nuclei) are created. If the alpha-decay continues because t(Ge81) = 7.6 s and the detachment of one more "A" particle takes place, then "olgoid" 77Zn will be synthesized. The equation of the reaction is 81Ge → 77Zn+4He. The yield of the products with a mass number of 77 is Y(77) = 0.008 (%), Table 3. It is this group, which the fragments 77Zn belong to, such a process can be defined as quaternary nucleus fission. The instance of the second process for light fragments can be the synthesis of fragments with an increased number of nucleons. Figure 5b contains the "olgoid" 112Ru obtained from the 101Zr fragment (Figure 3) after the capture of two "A" particles and three neutrons. The equation of the reaction is 101Zr+2·4He+3n → 112Ru. The yield of Y(112Ru) = 0.0099 (%) is in Table 3.

The instance of the first process for the heavy fragment can be that of the "olgoid" tin Sn127, as shown in Figure 6a, which is obtained from the 134Te fragment (Figure 3), having t(134Te) = 41.8 min and, in the case of decay with the detachment of one "A" particle and three neutrons, the equation of the reaction is 134Te → 127Sn+4He+3n. The yield of Y(127Sn) = 0.095 (%) is in Table 3. The instance of the first process for the heavy fragment can be that of the "olgoid" 155Nd, shown in Figure 6b, which is obtained from the 149Ce fragment (Figure 3) after capture of one "A"- particle and two neutrons. The equation of the reaction is 149Ce+4He+2n → 155Nd. The yield of Y(155Nd) = 0.018 (%) is in Table 3.
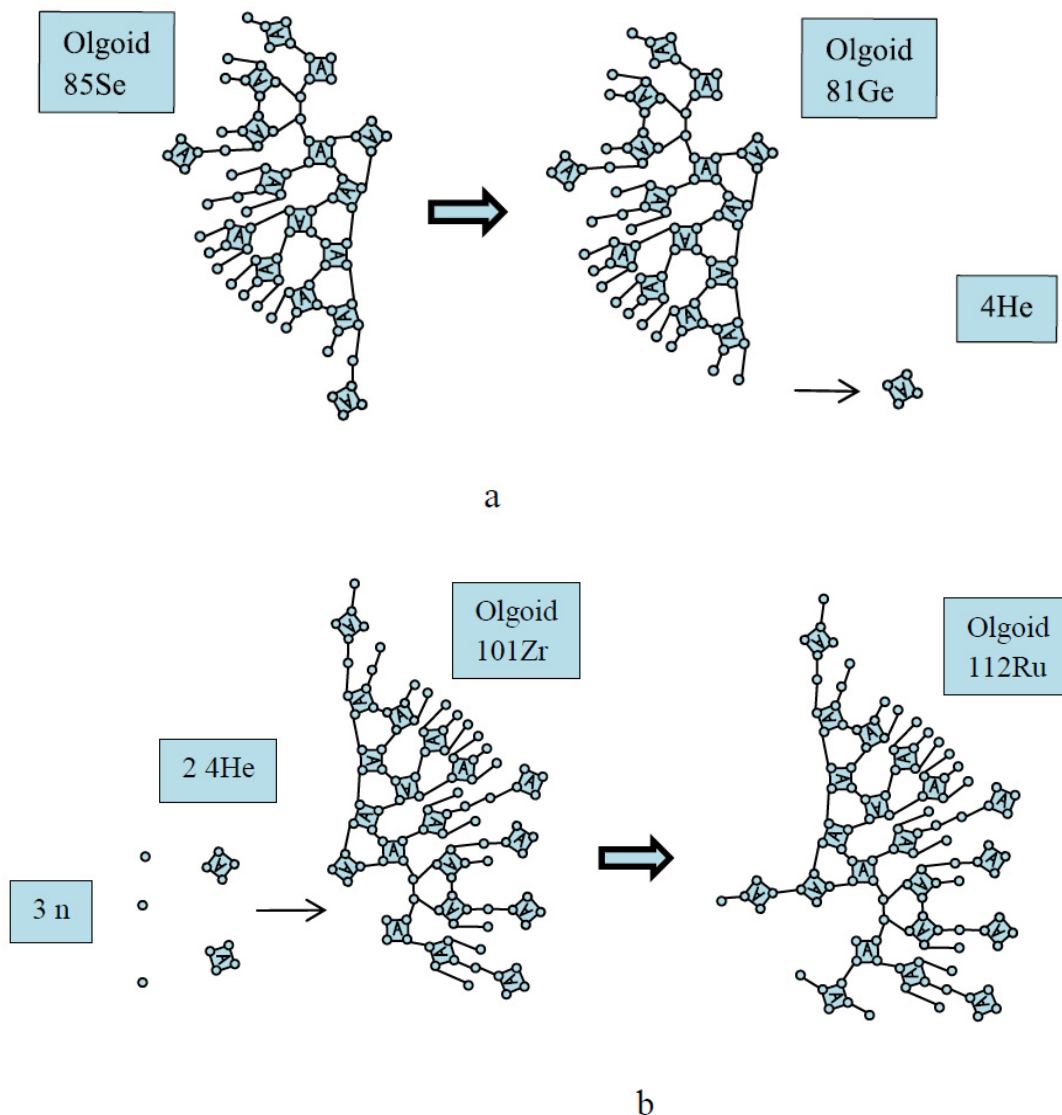
Figure 5. Fission of light fragment 85Se into 81Ge and 4He (**a**), synthesis of light fragment 112Ru from fragment 101Zr after capturing two alpha particles and three neutrons (**b**).

The data in Table 3 are represented graphically in Figure 7. The graphs show two curves, 1 and 2, that reflect qualitatively the fact that 235U+n fission into two equal parts is determined not only by the true binary division, but also by the contribution of synthesized light fragments (curve 1) and by the decay of heavy fragments (curve 2). The curves 1 (Figure 5b) and 2 (Figure 6a) visually qualitatively demonstrate how the probabilities of nuclear fission fragment yields are taken into account.

At the end of this section, we point out that today, many of the described nuclear reactions have not been experimentally observed. However, it does not mean that the probability of such reactions is zero.
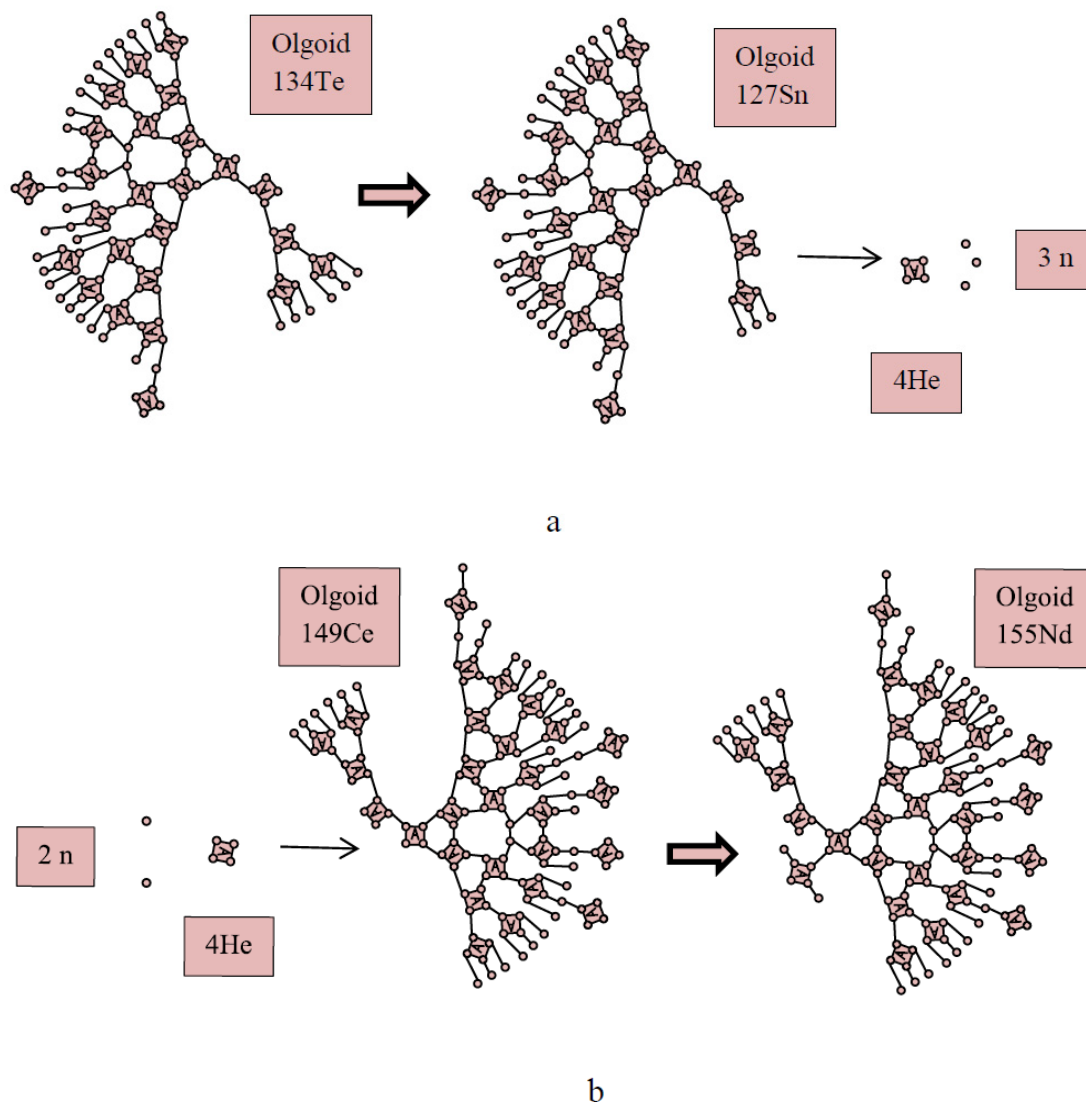
Figure 6. Fission of heavy fragment 134Te into 127Sn, alpha particle and three neutrons (**a**), synthesis of heavy fragment 155Nd from fragment 149Ce after capturing two neutrons and alpha particle (**b**).

3.3. Analysis of Fragment Binding Energy in the 235U+n Reaction

The described SMN model allows for predicting some results of future experiments. For instance, it is possible to consider the binding energy analysis for two light fragments of 92Rb_a a and 92Rb_b, whose "olgoids" are shown in Figure 8. Those nuclei are obtained in different reactions of the 235U_d nucleus fission along the lines B-B and B′-B′ (Figure 4) and have a different number of "A" particles, but the same numbers of nucleons.

The 92Rb_a fragment will have 18 "A" particles. It is obtained by the fission along the B-B line after the attachment of a thermal neutron to the left lobe and the detachment of three instantaneous neutrons from the right lobe. The 92Rb_b fragment will have 17 "A" particles. It is obtained by the fission along the B′-B′ line after the attachment of a thermal neutron to the right lobe of the "olgoid". Since the fraction of 92Rb fragments in the total isomer fission yield is relatively high Y(92Rb) = 6.01 (%), Table 3, the experiment will be provided with the quantity of the initial material. The difference in the binding energies between 92Rb_a and 92Rb_b is of several MeV. This follows from (1) and investigations of the number of "A" particles in the structures of different nuclei. It can be easily demonstrated on the experimental data for the known rubidium Rb isotopes, which have the greatest total percentage yield of various fission fragments.
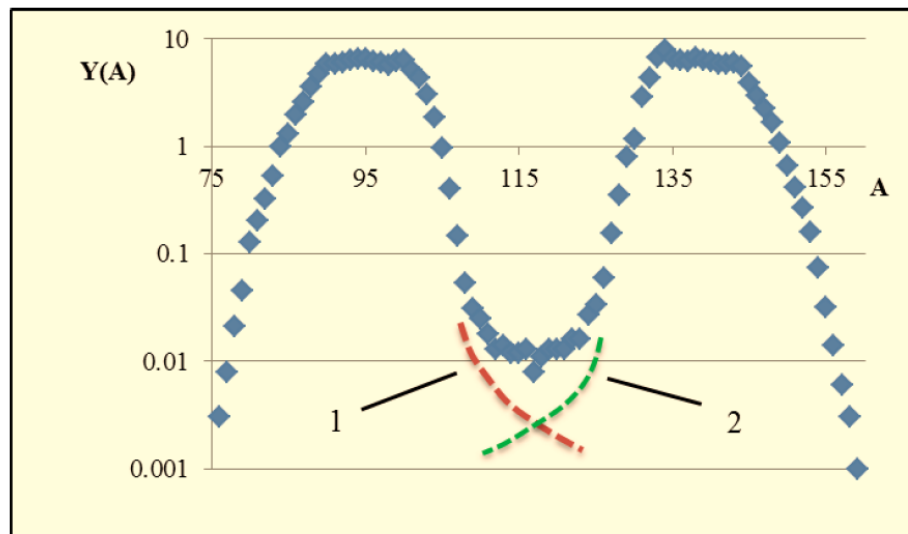
Figure 7. Fragment mass distribution after the 235U fission by thermal neutrons.
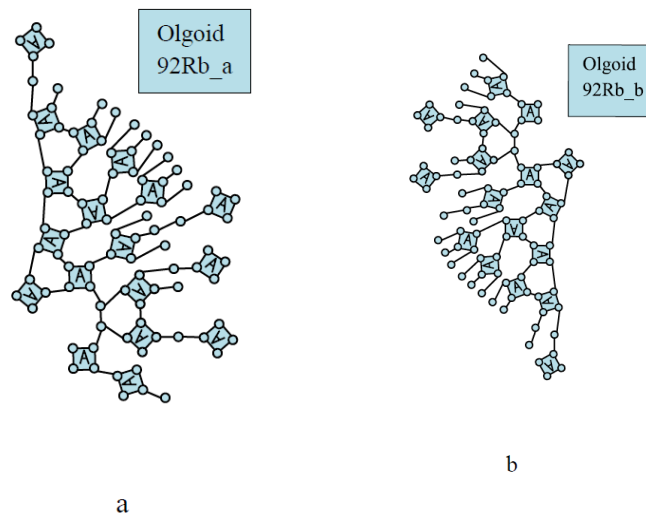

Figure 8. Structures of light fragments rubidium 92Rb_a (**a**) and 92Rb_b (**b**).

The structures of four isotope "olgoids", 85Rb, 87Rb, 89Rb and 91Rb, are presented in Figure 9. The 85Rb isotope is natural and its fraction is 72.17 (%) of the total rubidium quantity. This isotope has nucleus binding energy of $B_S(85Rb) = 739.282485$ (MeV). The 87Rb isotope is also natural and its fraction is 27.83 (%) of the total rubidium quantity. This isotope has nucleus binding energy of $B_S(87Rb) = 757.855521$ (MeV). The 89Rb isotope with excess neutrons has nucleus binding energy $B_S(89Rb) = 771.11291$ (MeV). The 91Rb isotope with excess neutrons has nucleus binding energy $B_S(91Rb) = 783.288324$ (MeV). For the same number of protons, $Z = 37$ and the same increase in the number of neutrons N by two ($N = 48, 50, 52$ and 54), the binding energy increases differently: $\Delta B_S(87Rb, 85Rb) = B_S(87Rb) - B_S(85Rb) = 18.573063$ (MeV); $\Delta B_S(89Rb, 87Rb) = 13.257389$ (MeV); $\Delta B_S(91Rb, 89Rb) = 12.175414$ (MeV).

The big difference in the binding energy increase between 85Rb and 87Rb can be explained by the change in the number of "A" particles. The 85Rb isotope has 16 "A" particles (Figure 9) and the 87Rb isotope has 17 "A" particles (Figure 9). An "A" particle always causes the biggest changes in the nucleus binding energy balance for any nucleus and that is reflected in (1). The 89Rb and 91Rb isotopes have the same number of "A" particles, which is equal to 17 (Figure 9). Therefore, two links of "C-type" slightly change

the average binding energy per link: $\Delta B_S(89Rb, 87Rb)/2 \approx 6.628$ (MeV); $\Delta B_S(91Rb, 89Rb)/2 \approx 6.088$ (MeV). This is less than the average binding energy for the link of "A-type" that is 7.074 (MeV) and this confirms absence of the "A" particle number increase. Contrary to that, the difference in the binding energy increase between 85Rb and 87Rb is approximately $\Delta B_S(87Rb, 85Rb) \approx 18.573$ (MeV) and it indicates the increase in the number of "A" particles by one in the structure of 87Rb, since the increase by 5–6 (MeV) is greater than $\Delta B_S(89Rb, 87Rb)$ and $\Delta B_S(91Rb, 89Rb)$. Such analysis contains one of the algorithms for determining the moment when the number of "A" particles in the nucleus structure changes. On the basis of this principle, the possible experiment on separation of fragments of 92Rb_a or 92Rb_b isotopes will be planned with respect to the difference in masses of several MeV (Figure 8) for different numbers of "A" particles, but the same number of nucleons. In this case, the result of the experiment will confirm the possibility of the SMN model to predict the differences in the binding energies for fission fragments with close numbers but different structures.
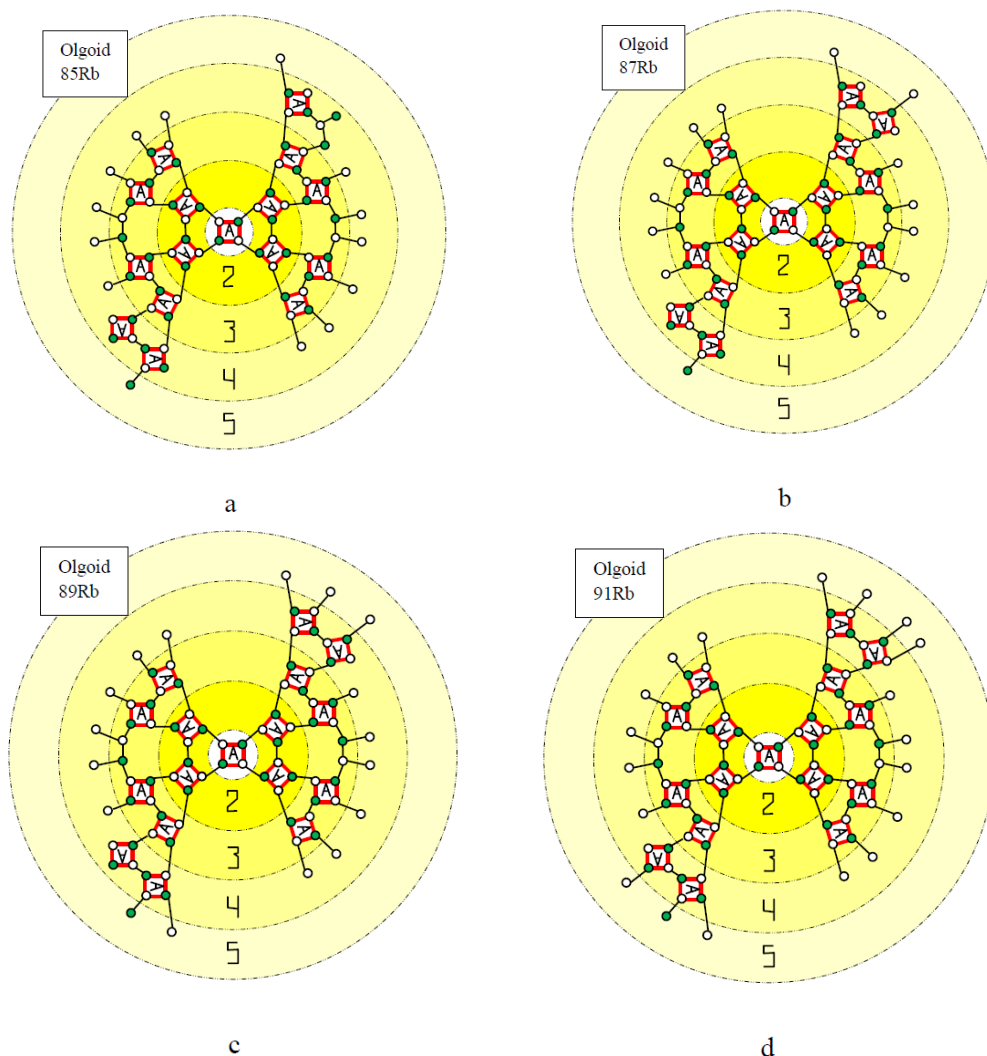

Figure 9. Structures of isotope nuclei of rubidium 85Rb (**a**), 87Rb (**b**), 89Rb (**c**) and 91Rb (**d**).

It is necessary to pay attention to the following additional result from our research. The 87Rb nucleus (Figure 9) is stable and is widely spread in nature, not owing to the "magic number" of neutrons $N = 50$ but to the fact that the structure of filling the nucleus layers by protons (the layers are marked with numbered circles) exactly corresponds to the filling of atom "electron shells" by electrons. It also complies with the periodic properties

of the D.I. Mendeleyev table. The main characteristics of "olgoids" 85Rb, 87Rb, 89Rb and 91Rb are represented in Table 1.

3.4. Conclusions Based on Investigations

1. The results of the research based on the proposed SMN model allow for determining all possible 235U+n nuclear fission variants, including improbable ones, and they completely agree with known experimental data. This confirms correctness of the developed principles and rules for a structural construction of an "olgoid", in which no one nucleon has more than three bindings with other nucleons.

2. The results of the calculation of the binding energies by means of expressions obtained within the framework of the SNM "olgoid" model, both qualitatively and quantitatively, agree with the results of the modern modifications of the droplet and shell models. This agreement covers the nuclei of all chemical elements.

3. For the first time, the number of alpha particles (N_A = 44) and the total number of bindings between nucleons (N_{cS} = 292) in 235U nucleus were established. Using the proposed method for the analysis of heavy nucleus fission, it is possible to unambiguously determine the fragments as the result of the fission along the lines B-B or B′-B′. The research results allow for determining 235U structures having the greatest fission energy efficiency.

4. The structural symmetry of all developed "olgoids" with respect to the center provides a physical explanation of stability and instability of heavy element nuclei. For instance, the complete symmetry of 238U, found in nature (Figure 10), ensures its high stability and prevalence in nature owing to weak ability for fission along the lines B-B and B′-B′. Therefore, in order to start the 238U+n nucleus fission, it is necessary at the first stage to add one neutron to it and obtain a non-symmetric 239U nucleus that is unstable and can participate in nuclear fission reactions. This approach is used in "breeder reactors".
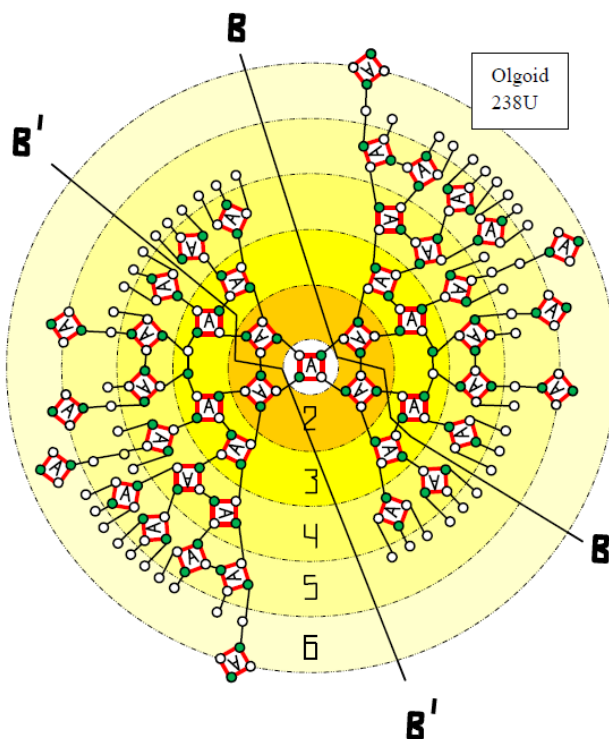

Figure 10. Structure of natural 238U nucleus.

References

1. Baba, H.; Takahashi, N.; Yokoyama, A.; Saito, T. Fast fission mechanism and duality of the diffusion process. *Eur. Phys. J.* **1998**, *3*, 281–292. [CrossRef]
2. Gontchar, I.; Morjean, M.; Basnary, S. Nuclear dissipation from fission time. *Eur. Lett.* **2002**, *57*, 355–361. [CrossRef]
3. Goutte, H.; Berger, J.F.; Casoli, P.; Gogny, D. Microscopic approach of fission dynamics applied to fragment kinetic energy and mass distributions in ^{238}U. *Phys. Rev. C* **2005**, *71*, 024316. [CrossRef]
4. Krappe, H.J. Cluster model versus Fermi-fluid approach to fission theory. *Int. J. Mod. Phys. E* **2007**, *16*, 396–401. [CrossRef]
5. Royer, G.; Bonilla, C. Multiple-humped fission and fusion barriers of actinide and superheavy elements. *J. Radioanal. Nucl. Chem. Artic.* **2007**, *272*, 237–242. [CrossRef]
6. Schmidt, K.-H.; Kelić, A.; Ricciardi, M.V. Experimental evidence for the separability of compoundnucleus and fragment properties in fission. *Eur. Lett.* **2008**, *83*, 32001. [CrossRef]
7. Sargsyan, V.V.; Kanokov, Z.; Adamian, G.G.; Antonenko, N.V. Quantum statistical effects in nuclear reactions, fission and open quantum systems. *Phys. Part. Nucl.* **2010**, *41*, 175–229. [CrossRef]
8. Umar, A.S.; Oberacker, V.E.; Maruhn, J.A.; Reinhard, P.G. Microscopic description of nuclear fission dynamics. *J. Phys. G Nucl. Part. Phys.* **2010**, *37*, 064037. [CrossRef]
9. Randrup, J.; Möller, P.; Sierk, A.J. Fission-fragment mass distributions from strongly damped shape evolution. *Phys. Rev. C* **2011**, *84*, 034613. [CrossRef]
10. Al-Adili, A.; Hambsch, F.-J.; Pomp, S.; Oberstedt, S. Impact of prompt-neutron corrections on final fission-fragment distributions. *Phys. Rev. C* **2012**, *86*, 054601. [CrossRef]
11. Schmidt, K.-H.; Jurado, B. Global view on fission observables–new insights and new puzzles. *Phys. Procedia* **2012**, *31*, 147–157. [CrossRef]
12. Aritomo, Y.; Chiba, S.; Ivanyuk, F. Fission dynamics at low excitation energy. *Phys. Rev. C* **2014**, *90*, 054609. [CrossRef]
13. Goriely, S. The fundamental role of fission during r-process nucleosynthesis in neutron star mergers. *Eur. Phys. J. A* **2015**, *51*, 22. [CrossRef]
14. Imanishi, N.; Fujiwara, I.; Nishi, T. Independent isomer yields of Sb and Te isotopes in thermal-neutron fission of 233U, 235U and 239Pu. *Nucl. Phys. A* **1976**, *263*, 141–149. [CrossRef]
15. Glendenin, L.E.; Gindler, J.E.; Henderson, D.J.; Meadows, J.W. Mass distributions for monoenergeticneutron-induced fission of ^{235}U. *Phys. Rev. C* **1981**, *24*, 2600–2605. [CrossRef]
16. Quade, U.; Rudolph, K.; Skorka, S.; Armbruster, P.; Clerc, H.-G.; Lang, W.; Mutterer, M.; Schmitt, C.; Theobald, J.; Gönnenwein, F.; et al. Nuclide yields of light fission products from thermal-neutron induced fission of 233U at different kinetic energies. *Nucl. Phys. A* **1988**, *487*, 1–36. [CrossRef]
17. Laurec, J.; Adam, A.; de Bruyne, T.; Bauge, E.; Granier, T.; Aupiais, J.; Bersillon, O.; Le Petit, G.; Authier, N.; Casoli, P. Fission Product Yields of 233U, 235U, 238U and 239Pu in Fields of Thermal Neutrons, Fission Neutrons and 14.7-MeV Neutrons. *Nucl. Data Sheets* **2010**, *111*, 2965–2980. [CrossRef]
18. Innes, M.M.; Chadwick, M.B.; Kawano, T. Fission product yields for 14 MeV neutrons on ^{235}U, ^{238}U and ^{239}Pu. *Nucl. Data Sheets* **2011**, *112*, 3135–3152. [CrossRef]
19. Schmitt, C.; Möller, P. On the isotopic composition of fission fragments. *Phys. Lett. B* **2020**, *812*, 136017. [CrossRef]
20. Pleasonton, F. Prompt γ-rays emitted in the thermal-neutron induced fission of ^{233}U and ^{239}Pu. *Nucl. Phys. A* **1973**, *213*, 413–425. [CrossRef]
21. Oberstedt, S.; Belgya, T.; Billnert, R.; Borcea, R.; Bryś, T.; Geerts, W.; Göök, A.; Hambsch, F.-J.; Kis, Z.; Martinez, T.; et al. Improved values for the characteristics of prompt-fission gamma-ray spectra from the reaction ^{235}U(n_{th},f). *Phys. Rev. C* **2013**, *87*, 051602(R). [CrossRef]
22. Vogt, R.; Randrup, J. Event-by-event study of photon observables in spontaneous and thermal fission. *Phys. Rev. C* **2013**, *87*, 044602. [CrossRef]
23. Zucker, M.S.; Holden, N.E. Energy Dependence of Neutron Multiplicity in Fast-Neutron-Induced Fission for ^{235,238}U and ^{239}Pu. In Proceedings of the American Nuclear Society Annual Meeting, Reno, NV, USA, 15 June 1986.
24. Naik, H.; Dange, S.P.; Singh, R.J. Angular momentum of fission fragments in low energy fission of actinides. *Phys. Rev. C* **2005**, *71*, 014304. [CrossRef]
25. Schmidt, K.-H.; Jurado, B. Final excitation energy of fission fragments. *Phys. Rev. C* **2011**, *83*, 061601. [CrossRef]

26. Maslov, V.M.; Tetereva, N.A.; Pronyaev, V.G.; Kagalenko, A.B.; Zolotarev, K.I.; Capote, R.; Granier, T.; Morillon, B.; Hambsch, F.-J.; Sublet, J.-C. 235U(n, f), 233U(n, f) and 239Pu(n, f) Prompt Fission Neutron Spectra. *J. Korean Phys. Soc.* **2011**, *59*, 1337–1342. [CrossRef]

27. Ebran, A.; Taieb, J.; Belier, G.; Chatillon, A.; Laurent, B.; Martin, J.-F.; Pellereau, E. Picosecond resolution on relativistic heavy ions time-of-flight measurement. *Nucl. Instrum. Methods Phys. Res. Sect. A Accel. Spectrometers Detect. Assoc. Equip.* **2013**, *728*, 40–46. [CrossRef]

28. Stetcu, I.; Talou, P.; Kawano, T.; Jandel, M. Isomer production ratios and the angular momentum distribution of fission fragments. *Phys. Rev. C* **2013**, *88*, 044603. [CrossRef]

29. Kadmensky, S.G. Mechanisms of binary and ternary low-energy fission of nuclei with allowance for nonsphericity effects. *Phys. Atomic Nucl.* **2004**, *67*, 170–182. [CrossRef]

30. Gönnenwein, F.; Tsekhanovich, I.; Rubchenya, V. Angular momenta of near-spherical fission fragments. *Int. J. Mod. Phys. E* **2007**, *16*, 410–424. [CrossRef]

31. Kadmensky, S.G. Quantum properties of deformation modes of fissile-nucleus motion. *Phys. At. Nucl.* **2008**, *71*, 1193–1199. [CrossRef]

32. Schmidt, K.-H.; Jurado, B.; Amouroux, C.; Schmitt, C. General Description of Fission Observables: GEF Model Code. *Nucl. Data Sheets* **2016**, *131*, 107–221. [CrossRef]

33. Kadmensky, S.G.; Lyubashevsky, D.E. Description of true and delayed ternary nuclear fission accompanied by the emission of various third particles. *Phys. At. Nucl.* **2010**, *73*, 1436–1442. [CrossRef]

34. Santhosh, K.P.; Krishnan, S.; Priyanka, B. Light charged particle accompanied ternary fission of 242Cm using the Coulomb and proximity potential. *Eur. Phys. J. A* **2014**, *50*, 66. [CrossRef]

35. Kadmensky, S.G.; Bulychev, A.O. Sequential character of low-energy ternary and quaternary nuclear fission. *Phys. At. Nucl.* **2016**, *79*, 793–797. [CrossRef]

36. Holmvall, P.; Köster, U.; Heinz, A.; Nilsson, T. Collinear cluster tri-partition: Kinematics constraints and stability of collinearity. *Phys. Rev. C* **2017**, *95*, 014602. [CrossRef]

37. Adamian, G.G.; Antonenko, N.V.; Bezbakh, A.N.; Malov, L.A. Manifestation of the structure of heavy nuclei in their alpha decays. *Phys. At. Nucl.* **2016**, *79*, 951–962. [CrossRef]

38. Kapitonov, I.M. *Vvedenie v Fiziku Yadra i Chastits: Textbook*, 5th ed.; Revised by Lenand, M.; 2017; 544p.

39. Cook, N.D. *Models of the Atomic Nucleus*; Springer: New York, NY, USA, 2010.

40. Ebran, J.-P.; Khan, E.; Nikšić, T.; Vretenar, D. Density functional theory studies of cluster states in nuclei. *Phys. Rev. C* **2014**, *90*, 054329.

41. Dubovichenko, S.B.; Burkova, N.A. Does the Excited Cluster 14N* Exist in the 15O Nucleus? *Russ. Phys. J.* **2019**, *61*, 2105–2112. [CrossRef]

42. Pauling, L. The Close-packed-spheron model of atomic nuclei and its relation to the shell model. *Proc. Natl. Acad. Sci. USA* **1965**, *54*, 989–994. [CrossRef]

43. Cook, N.D. LENR theory requires a proper understanding of nuclear structure. *J. Condens. Matter Nucl. Sci.* **2017**, *24*, 60–74.

44. Wigner, E. On the consequences of the symmetry of the nuclear Hamiltonian on the spectroscopy of nuclei. *Phys. Rev.* **1937**, *51*, 106. [CrossRef]

45. Sukhanov, A.D. *Lektsii po kvantovoi fizike: Teaching Aid*; Sukhanov, A.D., Golubeva, O.N., Eds.; Vysshaya shkola: Moscow, Russia, 2006; 528p.

46. Nordling, C.; Osterman, J. *Physics Handbook for Science and Engineering*, 8th ed.; Professional Publishing House: Los Angeles, CA, USA, 2006; p. 503.